

Screening Mammography Breast Cancer Detection

Debajyoti Chakraborty
Northeastern University
360 Huntington Ave, Boston, MA 02115
chakraborty.de@northeastern.edu

Abstract

Breast cancer is a leading cause of cancer-related deaths, but current programs are expensive and prone to false positives, leading to unnecessary follow-up and patient anxiety. This paper proposes a solution to automated breast cancer detection, to improve the efficiency and accuracy of screening programs. Different methodologies were tested against the RSNA dataset of radiographic breast images of roughly 20,000 female patients and yielded an average validation case pF1 score of 0.56 across methods.

1. Introduction

Breast cancer is one of the most commonly occurring cancer in the world with 2.3 million new breast cancer diagnoses and 685,000 deaths in 2020 alone [6]. Although the mortality rate in developed nations have dropped by 40% over the last 40 years due to regular mammography screening programs, such is not the case in many other countries due a looming shortage of radiologists.

As with any cancer or disease in general, early detection and treatment is critical to reducing complications and fatalities. However, currently such procedures require the expertise of highly-trained human observers, primarily radiologists, making the overall process expensive to conduct and prone to human error, worsening the problem.

2. Problem Statement

A major problem in mammography screening is that it often leads to a high incidence of false positive results. This is usually followed by further screening tests, inconvenient follow-up, and sometimes, unneeded tissue sampling (needle biopsy) which may lead to further unrelated complications, causing unnecessary anxiety.

This paper aims to improve the automatic detection of breast cancer in screening mammograms obtained from regular screening programs, with the goal being to reduce the occurrences of false positives in a clinical setting.

2.1. Dataset

[This dataset contains radiographic breast images of female subjects.]

The dataset [2] has been generously provided by the Radiological Society of North America (RSNA). RSNA is a non-profit organization that represents 31 radio-logic specialties from 145 countries around the world.

It contains radiographic breast images of roughly 20,000 female patients with usually four images per patient with two lateral [left, right] images per view [mediolateral-oblique (MLO), crinal-caudal (CC)].

Table 1. Metadata for each patient and image

site id	ID code for the source hospital
machine id	ID code for the imaging device
patient id	ID code for the patient
image id	ID code for the respective image
laterality	whether the image is of the left or right breast
view	orientation of the image
age	patient's age in years
implant	whether the patient had breast implants at the patient level
density	rating for how dense the breast tissue is, with A being the least dense and D being the most dense
biopsy	whether a follow-up biopsy was performed on the breast
invasive	whether or not the cancer (if true) proved to be invasive
BIRADS	0 if the breast required follow-up, 1 if the breast was rated as negative for cancer, and 2 if the breast was rated as normal
difficult negative case	true if the case was unusually difficult to diagnose
cancer	whether or not the breast was positive for malignant cancer

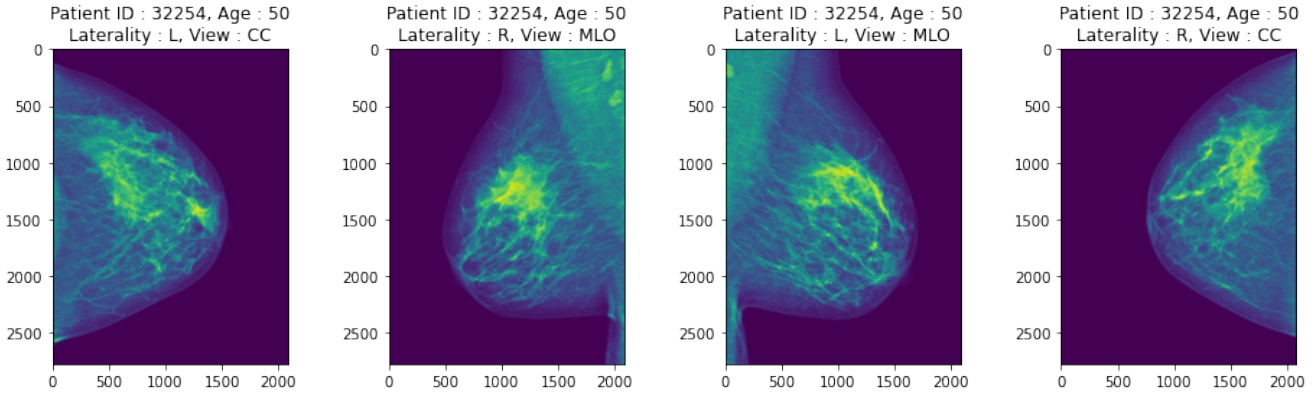


Figure 1. Example MLO and CC view of left(L) and right(R) breasts for patient id 32254.

The raw dataset contains around 54,700 mammography images in the Digital Imaging and Communications in Medicine (DICOM) [4] format. There is a significant class imbalance in the target variable *cancer*, with 1,158 data-points for the positive class and 53,548 data-points for the negative class. For the purpose of this paper, *image id* serves as the input data, *cancer* as the binary target, along with only *age* and *implant* information as additional metadata. The rest of the metadata will be included in a future implementation for better inference.

3. Approach

3.1. Image encoding

Majority of the work was involved in pre-processing the DICOM images and converting them into png files for easier post-processing and training. Most of the dicoms in the dataset contained JPEG2000 encoded images. The bit-stream was extracted and decoded on the GPU, saved as png files. Although this process was not lossless, it saved a lot of overhead for processing them individually, as they were quite high-dimensional.

3.2. Pre-processing

Different pre-processing techniques were tried to improve the chances of accurate classification. Two of the primary techniques were Region of Interest ROI cropping and normalization. However, upon further research, it was only decided to use normalization and drop cropping, due to the variability in image dimensions and loss of information by resizing. Photometric interpretation, an attribute that specifies the intended interpretation of the raw pixel data were either MONOCHROME1 or MONOCHROME2. MONOCHROME1 is usually used when the mammogram is intended to be viewed in a **white** background and MONOCHROME2 is usually used when the mammogram is intended to be viewed in a **black** background. The author chose to invert all

MONOCHROME1 images and keep all MONOCHROME2 images intact, as they display more lesion-based information when viewed by a machine. All original image arrays were normalized to between 0 and 1 for uniformity, and resized into 512×512 gray-scale images for consistency.

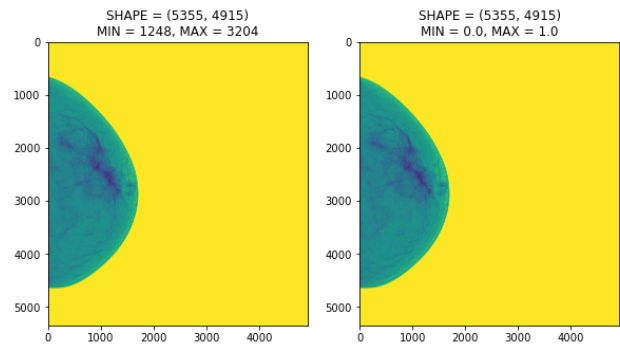


Figure 2. (left) Random sample of a MONOCHROME1 image showing the minimum pixel value and (right) the same image after inverting and normalizing all pixel values to between 0 and 1.

3.3. Feature extraction

An EfficientNetV2 [8] with pre-trained weights was used to extract essential features from the images, encoding them to a 1000-dimensional feature vector. It was developed by researchers at Google [3] that achieved improved accuracy and efficiency than conventional Convolutional Neural Networks (CNNs), lowering parameter size and execution time by an order of magnitude.

An modification of the dataset was later prepared by combining the exported image feature vectors with two meta features: normalized **age** and **implant** information. For the purpose of improving predictions, a combination of synthetic under-sampling and over-sampling techniques were also tested for performance. [1].

3.4. Classification methods

These popular machine learning techniques for classification were trained on this data to derive inference.

3.4.1 Logistic Regression (LR)

A simple LR model with L2 regularization was trained on the unbalanced dataset with individually assigned class weights and has been described below.

Given X_i as the input feature vector and $y_i \in \{0, 1\}$ as the target variable for data point i , the probability of the positive class $y_i = 1$ was predicted by the fitted model as:

$$\hat{p}(X_i) = P(y_i = 1|x) = \frac{1}{1 + \exp(-X_i w - w_0)} \quad (1)$$

The cost function that was minimized using a solver was:

$$\min_w C \sum_{i=1}^{N_n} (-y_i \log(\hat{p}(X_i)) - (1 - y_i) \log(1 - \hat{p}(X_i))) + \frac{1}{2} \|x\|_2^2 \quad (2)$$

3.4.2 Support Vector Machine (SVM)

For implementing a SVM model, a scalable, input data independent polynomial kernel approximation method [7] was used. Given x, y as input features and d as the polynomial kernel degree, a simple kernel function used was:

$$k(x, z) = (\gamma x^\top z + c_0)^d \quad (3)$$

Next, given that $X_i \in \mathbb{R}^d$ and $y_i \in \{-1, 1\}$ as the target variable for data point i , the following problem was solved:

$$\begin{cases} \min_{w,b,\xi} \frac{1}{2} \|w\| + C \sum_{i=1}^n \xi_i \\ \text{such that } y_i (w^\top k(x, z) + b) \geq 1 - \xi_i \\ \xi_i \geq 0, \quad \forall i = 1, \dots, n \end{cases} \quad (4)$$

Equivalently formulated, it was written as:

$$\min_{w,b} \frac{1}{2} \|w\| + C \sum_{i=1}^n \max(0, 1 - y_i (w^\top k(x, z) + b)) \quad (5)$$

3.4.3 Breast-level single-view-single-laterality model

A simple deep-neural network was designed to perform inference on the ensemble of features described above.

- **Input:** Each 1000×1 vector was fed into an **image encoder** part of the network and after two hidden dense layers was concatenated with the feature outputs from a **metadata encoder**.

- **Activation:** Each intermediate layer had a **ReLU** activation function, except for the output layer, where a **Sigmoid** activation was used.

$$\text{ReLU: } f(z) = \max(0, z) \in [0, z] \quad (6)$$

$$\text{Sigmoid: } f(z) = \frac{1}{1 + \exp(-z)} \in [0, 1] \quad (7)$$

- **Loss:** The loss with respect to the target variable was calculated using **Binary Cross-entropy (BCE)** loss, once while using categorical class weights and another without.

$$- \frac{1}{N} \sum_{i=0}^N y_i \log(\hat{y}_i) + (1 - y_i) \log(1 - \hat{y}_i) \quad (8)$$

- **Class imbalance:** In the latter case, a **Straified Batch Sampling (SBS)** methodology was used when randomly sampling from the dataset during training.

$$\text{SBS} = \frac{\text{Total sample size}}{\text{Dataset population}} \times \text{Class population} \quad (9)$$

- **Optimizer:** Adam [5] was chosen as the optimizer for our minimization problem. Given $\eta = 0.0003$ as initial learning rate, g_t as gradient at time t along w_j , ν_t as exponential average of gradients along w_j , s_t as exponential average of squares of gradients along w_j and β_1, β_2 as hyper-parameters:

$$\nu_t = \beta_1 \nu_{t-1} - (1 - \beta_1) g_t \quad (10)$$

$$s_t = \beta_2 s_{t-1} - (1 - \beta_2) g_t^2 \quad (11)$$

$$\partial w_t = -\eta \frac{\nu_t}{\sqrt{s_t + \epsilon}} g_t \quad (12)$$

$$w_{t+1} = w_t + \partial w_t \quad (13)$$

- **Metrics:** A range of different metrics were tried to understand the maximum efficiency of the model. As for a problem with a class imbalance, **accuracy** was unreliable because of the major bias towards negative class. In this regard, performances of binary area under the receiver operating characteristic curve (AUROC), binary precision, binary recall, binary F_1 score were compared. A comprehensive comparison of these metrics have been provided in Figure 3.

The model was finally evaluated using the **probabilistic F_1 score** (pF_1) [9] as this extension accepts probabilities instead of binary classifications. With p_x as the probabilistic version of X :

$$pF_1 = 2 \frac{P_{\text{precision}} P_{\text{recall}}}{P_{\text{precision}} + P_{\text{recall}}} \quad (14)$$

$$P_{\text{precision}} = \frac{P_{\text{true positive}}}{P_{\text{true positive}} + P_{\text{false positive}}} \quad (15)$$

$$P_{\text{recall}} = \frac{P_{\text{true positive}}}{\text{true positive} + \text{false negative}} \quad (16)$$

Table 2. Simple Single-view-single-laterality model architecture

Layer	Input	Output	Parameters
SimpleFCN	[,1002]	[,1]	–
Sequential: 1-1	[,1000]	[,10]	–
Linear: 2-1	[,1000]	[,100]	100, 100
ReLU: 2-2	[,100]	[,100]	–
Linear: 2-3	[,100]	[,10]	1, 010
ReLU: 2-4	[,10]	[,10]	–
Linear: 2-3	[,10]	[,1]	11
Sigmoid: 2-4	[,1]	[,1]	–
Sequential: 1-2	[,2]	[,1]	–
Linear: 2-5	[,2]	[,2]	6
ReLU: 2-6	[,2]	[,2]	–
Linear: 2-7	[,2]	[,1]	3
Sigmoid: 2-8	[,1]	[,1]	–
Concatenate: 1-3	[,2]	[,1]	–
Sigmoid: 1-4	[,1]	[,1]	–

The total parameters in the model was estimated at 101, 130, all of which were trainable. The total model size excluding the feature extractor was estimated at 20.56 MB, with input size at 16.42 MB, forward/backward pass size at 3.74 MB and all parameter size at 0.40 MB.

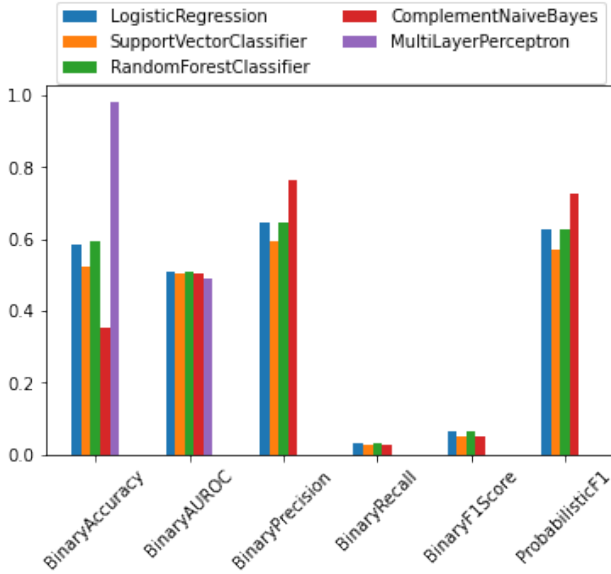


Figure 3. Comparison of different evaluation metrics.

4. Results

An extensive array of experiments were carried out to estimate the best machine learning model suited for this dataset. This not only included varying hyper-parameters and trying out different models, but also making efforts in transforming, augmenting and generating synthetic data points for the imbalanced classes.

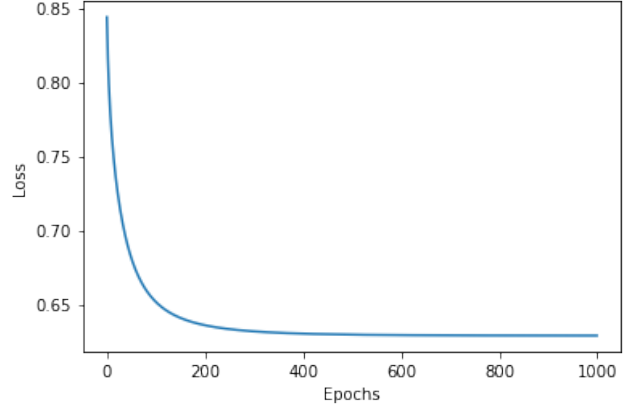


Figure 4. Validation loss graph trained for 1000 iterations with breast-level single-view-single-laterality DNN model.

The results for pF_1 score were compared as well in order to have a more holistic view at all the approaches, and served well to gauge different model performances compared to each other and state of the art at present. This was due to lack of good test data, lack of sufficient positive classes, and personally, lack of time and resources.

Table 3. Probabilistic F-1 scores

Model	pF_1 score
State-of-the-art	0.630
Logistic Regression	0.627
Support Vector Machine	0.572
Random Forest Classifier	0.626
Complement Naive Bayes	0.579
Deep Neural Network	0.481

5. Summary

As it can be inferred from the above table, the current state of any of the models is not better than 0.50 probability, that is a 50% chance of providing the correct class prediction, which is not any better than random chance. Comparing the results to the current state-of-the-art shows that the topic needs more correct predictions to be relevant.

Other investigations that did not produce significant results include Region-of-interest (ROI) cropping, down-

sampling, up-sampling or synthetically generating new samples for the dataset, and almost certainly leading to over-fitting. The rest of the metadata was not part of future test samples, so they were not included as well.

Literature survey shows that the use of intense data augmentation pipelines and training models externally on similar datasets work well. This is mainly done to lessen the possibility of detection of false positives due to exposure to more data points in the positive class. There is also strong evidence that networks that capture both spatial and temporal information for a single patient, in a multi-view-multilateral model show drastically improved performance. The recent use of transformers for vision tasks has shown significant promise as well, but that calls for further investigation and is also outside the scope of this paper.

References

- [1] Mateusz Buda, Atsuto Maki, and Maciej A. Mazurowski. A systematic study of the class imbalance problem in convolutional neural networks. *Neural Networks*, 106:249–259, oct 2018. [2](#)
- [2] George Partridge inversion Jayashree Kalpathy-Cramer John Mongan Katherine Andriole Lavender Maryam Vazirabad Michelle Riopel Robyn Ball Sohler Dane Yan Chen Chris Carr, Felipe Kitamura. Rsna screening mammography breast cancer detection, 2022. [1](#)
- [3] Mingxing Tan [Staff Software Engineer and Google AI] Quoc V. Le, Principal Scientist. EfficientNet: Improving Accuracy and Efficiency through AutoML and Model Scaling, 5 2019. [2](#)
- [4] Llc Innolitics. Digital Mammography X-Ray Image CIOD. [2](#)
- [5] Diederik P. Kingma and Jimmy Ba. Adam: A method for stochastic optimization, 2017. [3](#)
- [6] World Health Organization. World health organization: Who. (2021). breast cancer., 2021. <https://www.who.int/news-room/fact-sheets/detail/breast-cancer>. [1](#)
- [7] Ninh Pham and Rasmus Pagh. Fast and scalable polynomial kernels via explicit feature maps. In *Proceedings of the 19th ACM SIGKDD International Conference on Knowledge Discovery and Data Mining*, KDD '13, page 239–247, New York, NY, USA, 2013. Association for Computing Machinery. [3](#)
- [8] Mingxing Tan and Quoc V. Le. Efficientnetv2: Smaller models and faster training, 2021. [2](#)
- [9] Reda Yacouby and Dustin Axman. Probabilistic extension of precision, recall, and f1 score for more thorough evaluation of classification models. In *Proceedings of the First Workshop on Evaluation and Comparison of NLP Systems*, pages 79–91, Online, Nov. 2020. Association for Computational Linguistics. [3](#)